# Cost-effective sizing of a Hybrid Regenerative Hydrogen Fuel Cell Energy Storage System for Remote & Off-Grid Telecom Towers

Gerard Jansen*[,a], Zahir Dehouche[a], Harry Corrigan[b]

[a] *Centre for Energy and Built Environment Research, Brunel University London, United Kingdom, UB8 3PH, UK*
[b] *SolarBotanic Ltd. 2SolarBotanic Ltd, Kemp House 152 City Road, London EC1V 2NX, UK*

*Corresponding author e-mail: Gerard.Jansen@brunel.ac.uk , phone: +44 (0)7534 077 847

## Abstract

There is an urgent need to provide cost-effective, clean, distributed electricity to ensure reliability for mobile network operators in Sub-Saharan Africa. A comprehensive semi-empirical MATLAB/Simulink model of a novel low-pressure, solid-hydrogen based energy storage system combined with Solar PV and battery energy storage including dynamic losses of the power conditioning equipment is built. Levenburg-Marquardt least square algorithm is used for semi-empirical parameterisation of the metal-hydride and fuel cell models, simulations are performed using experimentally obtained telecom tower load data. The results show the overall system efficiency of the energy system drop from 21.05% for a Solar/Battery system to 17.43% of the most cost-effective hybridised system, which consists of 16.2 kW Solar PV coupled to a 10kW/40kWh Li-Ion battery, and a Regenerative Hydrogen Fuel Cell (consisting of a 10kW PEM Electrolyser, 1,000kWh Ti-based AB2 Solid-Hydrogen Storage Cell, and 5kW PEM Fuel Cell). This system achieves a Levelised Cost of Electricity of 17.16 ¢/kWh compared to 73.40 ¢/kWh for a Diesel Genset, with a Net Present Value of $109,236 and an Internal Rate of Return of 15.15%.

## Highlights

1. Solid-hydrogen storage for a single tenant, off-grid telecom tower is proposed.
2. Semi-empirical parameterisation of Fuel Cell and Metal-Hydride are presented.
3. Hybridising Li-Ion and hydrogen energy storage increases economic viability.
4. Levelised Cost of Electricity of 17.16 ¢/kWh, Internal Rate of Return of 15.15%.

Keywords: Energy Storage, Hydrogen, Fuel Cell, Electrolyser, Metal-Hydride, Energy system

## Nomenclature

| | |
|---|---|
| $A$ Area ($m^2$) | $K_i$ Current temperature coefficient (A/°C) |
| $C_t$ Capital expenditures ($) | $M_t$ Operation and Maintenance expenditures ($) |
| $E_{act}$ Activation overpotential (V) | M Metal reaction site |
| $E_{ohm}$ Ohmic overpotential (V) | $n$ Number of electrons in reaction |
| $E_{conc}$ Concentration overpotential (V) | $N_P$ Number of cells in parallel |
| $E_{g0}$ Band gap energy of silicon semiconductor (eV) | $N_S$ Number of cells in series |
| $E_t$ Electricity generated (kWh) | $O_2$ Oxygen molecule |
| $F$ Faraday constant (C/mol) | $P_{eq}$ Equilibrium pressure (atm) |
| $f_{H_2}$ Molar flow rate (mol/s) | $q$ Electron charge (C) |
| $F_t$ Fuel expenditures ($) | $R$ Resistance (Ω) |
| $G$ Solar irradiance (W/$m^2$) | $R_i$ Internal resistance (Ω) |
| $H^+$ Hydrogen proton | $R_S$ Series resistance (Ω) |
| $H_2$ Hydrogen molecule | $R_{SH}$ Shunt resistance (Ω) |
| $H_2O$ Water molecule | $S$ Stoichiometric ratio |
| $i$ Operating current density (A/$cm^2$) | $T$ Temperature (˚C) |
| $i_L$ Limiting current density (A/$cm^2$) | $T_{ref}$ Reference temperature (˚C) |
| $I$ Operating current (A) | $V$ Operating voltage (V) |
| $I_0$ Dark saturation current of Solar PV (A) | $V_{Nernst}$ Nernst voltage (V) |
| $I_{SC}$ Short circuit current (A) | $V_{OC}$ Open circuit voltage (V) |
| $I_{RS}$ Reverse saturation current (A) | $V_T$ Thermal voltage Solar PV (V) |
| $I_{PH}$ Photo-current of Solar PV (A) | $\alpha$ Charge transfer coefficient |
| $I_{PV}$ Operating current of Solar PV (A) | $\eta$ Overall efficiency (%) |

| | |
|---|---|
| $I_{SH}$ Shunt current of Solar PV (A) | $\eta_F$ Faraday efficiency (%) |
| $k$ Boltzmann's constant (J/K) | $\gamma$ Voltage temperature coefficient (V/°C) |

# 1. Introduction

Mobile telecommunication is changing rapidly in Sub-Saharan Africa. The Groupe Speciale Mobile Association (GSMA) predicts an annual growth of 4% in unique subscribers over the next decade [1], which enables access to life-enhancing services through simple connection between individuals, information, markets and services [2]. Chavula showed fixed- and mobile telephony and internet connection to have a significant impact on people's living standard and per capita income growth in the upper-middle-income countries, while only mobile telephony has a significant impact on growth in the upper-low-income and low-income countries in Africa [3]. Additionally, in 2017 the mobile telecommunication ecosystem contributed to 6.5% of the Gross Domestic Product (GDP) of the West African economy [1]. To serve the 190 million extra mobile phone subscriptions [4], Sub-Saharan Africa (SSA) will have an expected total of 66,200 bad-grid and off-grid towers in operation by 2020 [5].

The reliability of these telecom facilities, as well as its energy management, is critical for telecom operators. In absence of grid-based electricity, diesel generators (Gensets) are typically used to provide uninterrupted power supply to the telecom equipment. On-site energy generation and consumption for these telecommunication tower sites has become the largest operational expenditure (OPEX) for Mobile Network Operators (MNOs). Historically, MNOs main focus was on ensuring uptime and at that time, diesel was considered the only effective power source that could achieve acceptable levels. As a result, more than 95% of off-grid and bad-grid tower sites is powered by oversized Diesel Gensets (typically over 15kVA) [5]. Diesel Gensets are considered as one of the major sources of greenhouse gas pollutants and are known to cause several respiratory health issues as well [6]. In Nigeria alone, over 500 million litres of diesel are consumed on telecommunication tower sites, cumulatively emitting 1.3 million metric tonnes of $CO_2$ annually [7]. Some of the additional challenges faced by MNO's using this inefficient, and polluting energy solution include high mean time to repair, increasing fuel cost and consumption, high operational cost, high cooling load, fuel theft, and environmental pollution (oil spillage and noise) [8]. Thereby, the high OPEX results in cost of electricity at off-grid sites that can rise up to US$2.21 per kWh; about 10 to 20 times the price of electricity from the grid in most African countries [5]. This means that, on an off-grid site, over 30% of OPEX is directly allocated to diesel cost and logistics [9]. Additionally, failure of diesel generators is responsible for 65% of the loss of telecom service [10]. Hence, the need for alternative power sources providing cost-effective, clean, and resilient electricity is urgent to ensure reliability in the mobile network.

## 1.1 Literature review

Several studies have investigated the use of renewable energy technologies for powering telecommunication towers, either with energy storage, fossil fuel, or a combination to balance the intermittency. Oviroh and Jen examined the use of various solar hybrid system operating schedules in comparison to diesel generator operating schedules in powering several telecommunication towers sites across Nigeria. Their findings show that a hybrid Solar PV, combined with diesel generator, provided lowest levelised cost of electricity (LCOE), as low as 15.6 ¢/kWh [8]. Olatomiwa et al. found comparable results when assessing hybrid PV/Diesel/Battery and PV/Wind/Diesel/Battery power systems [7]. Khan et al. used HOMER software to simulate several Solar PV/Wind/Diesel/Battery configurations to find that the LCOE is lowest for Solar PV/Diesel/Battery at 16.2 ¢/kWh [11].

Besides diesel and battery energy storage, hydrogen also gains interest as a storage technology for remote telecommunication tower sites. Hydrogen storage in a Regenerative Hydrogen Fuel Cell (RHFC) utilizes on-site hydrogen generation through electrolysis, hydrogen storage, and electricity generation through a fuel cell. Recent advances in the electrolysis process have increased efficiencies of $H_2$ generation from water. Thereby, progress in manufacturing processes, as well as increased market maturity and acceptance have reduced capital costs [12], consequently enhancing its feasibility for use in remote telecommunication towers. RHFC's provide several advantages over conventional batteries. Batteries have a limited life expectancy between 3-8 years, their capacity diminishes over time and deep discharge cycles can damage the battery. Fuel Cells are more predictable with runtimes longer than 8 hours and last over 10 years [13, 14]. Thereby, an RHFC offers the ability to independently configure storage capacity, power output and recharge time.

Simulations performed by Amutha & Rajini indicate that a hybrid system comprising of Solar PV/Wind/Battery or Solar PV/Wind/Battery/FC can be feasible for telecommunication tower sites [15]. Additionally, Serincan performed empirical tests to successfully prove the commercial viability of a fuel cell system with respect to its lifetime [16]. This is backed up by Scamman et al., who investigated the use of hydrogen energy storage to reduce the number of batteries required and extend the batteries lifetime [17]. Focussing on the LCOE, Guinot et al. combined 35 bar hydrogen storage to a PV/Battery system and estimated cost reduction of 10% due to reduced energy storage capacity of the costly battery pack [18].

At ambient temperature and pressure, one gram of hydrogen occupies 11 litres [19]. Therefore, storage of hydrogen faces challenges to make it economic, efficient and safe [20]. High-pressure hydrogen gas storage is used in the before mentioned studies. Compressing hydrogen to a pressure of 200-700 bar increases the hydrogen density from 11 g/L to 22.9 g/L at 350 bar [21] and 39 g/L at 700 bar [22], thereby reducing space requirements. Due to the chemical properties of hydrogen and the required high pressures, compression is often costly and usually has a high energy demand. Hydrogen storage is also possible in metal-hydride at low pressure by chemisorption in e.g. magnesium- [23], or titanium-based [24] metallic compositions in solid-state, or by molecular physisorption on activated carbon [25], making it a safer, more convenient method [26]. Metal-Hydride storage uses the reversible chemical process of reaction between a crystal-structured solid metal with hydrogen gas. When hydrogen encounters the surface of the metal, the hydrogen molecule splits into two individual hydrogen atoms which are absorbed into the crystal structure of the metal to form a metal-hydride. The process of absorption is called the hydriding process, and heat is released as a result of the exothermic reaction. When heat is applied to the metal-hydride, the hydrogen is released as a gas during the de-hydriding process. Both the hydrogen and metal return to their original phase and the reaction is therefore reversible [27]. Compared to the volumetric energy density of gaseous (4.4 MJ/L) and cryogenic (8.4 MJ/L), metal-hydride can deliver a volumetric energy density of up to 13 MJ/L [28]. The use of metal-hydrides in remote telecom applications is particularly interesting, as the high energy density reduces space requirements, and the lower operating pressures mitigate the safety risks to personnel during maintenance activities.

## 1.2 Contribution

In this study, the technical and economic viability of hydrogen storage in solid-state is evaluated for use as energy storage technique to provide backup power to remote telecommunication towers. A particular focus is laid on rural, Sub-Saharan telecommunication that currently heavily rely on delivery of diesel fuel to operate reliably. Therefore, the water consumption and production in the closed RHFC is considered, to analyse the advantages of water recovery and recirculation with respect to the autonomous operation in rural areas where clean water is scarce, and delivery is challenging. In particular, this study uses a comprehensive semi-empirical MATLAB/Simulink model, establishes a strong evidence-based data set and formulate possible integration options of a novel low-pressure, solid-state hydrogen-based energy storage system combined with Solar PV and battery energy storage, including dynamic losses of the power conditioning equipment. Levenburg-Marquardt least square algorithm is used for semi-empirical parameterisation of the metal-hydride and fuel cell models and the design parameters are presented. Additionally, simulations are performed using experimentally obtained telecom tower load data which is also presented in this paper.

The methodology section explains the system's components of the analysed energy system topologies. The control logic of the system is shown to understand the decision making, and the technical parameters that are used for the system design are presented. Following that, the semi-empirical MATLAB/Simulink model is described, and the input parameters are given. To understand better the impact of hybridisation of lithium-ion battery with the solid-hydrogen energy storage system, several system configurations are analysed to find the impact on important financial parameters that can prove the system cost-effective. These results of the technical feasibility and economic viability are presented and to conclude, future improvements and research efforts are presented.

# 2. Methods

The assessment of the technical feasibility and cost-effective sizing of the energy system is performed using MATLAB/Simulink. The simulation model is based on energy and power balances and discretized according to the input data. Energy data results are extracted for further economic assessment in MS Excel.

## 2.1 System components characteristics

The choice of the right technology for primary and backup power supply for optimum performance of the telecommunication site depends on several factors such as site space, site location, load profile, natural surroundings, etc. Nigeria's climate offers the opportunity to deploy distributed solar PV, since capacity factors can reach as high as 19.2% [29].

The Solar PV array consists of SunPower X22-360-COM [30] modules connected in parallel, as individual module voltage of 59.1V is already sufficient for battery storage in a 48VDC nominal battery circuit, and the wiring circuitry is sufficiently short to avoid big voltage drop due to the high nominal operating current of 240A. Consequently, the MPPT DC/DC converter tracks the maximum power point to ensure efficient electricity generation. Because of the non-dispatchable, intermittent nature of solar energy and the dependency on atmospheric conditions, solar-based power systems must employ an energy storage system [31].

There are several technologies available for energy storage. Batteries are a typical solution for short term energy storage since they are highly efficient and have established supply chains, but the limited runtime, temperature sensitivity and disposal are just a number of challenges faced [32]. Batteries also face theft and vandalism issues; cell site operators report that battery theft is almost as acute a problem as diesel theft [33]. Hydrogen is considered as a viable alternative for the surplus energy storage from renewable sources [10, 34, 14, 35]. Although the Capital Expenditures (CAPEX) of hydrogen technologies is above that of competing technologies, the reduced OPEX and long lifetime stability make it a cost-efficient solution for their use in stand-alone telecommunication tower applications [15, 17, 18]. However, the process of power-to-hydrogen-to-power results in low Round-Trip-Efficiency (RTE). Hence a hybrid between high-efficient Lithium-Ion batteries short-duration storage and cost-effective fuel cell for long-duration storage is favourable [36, 37].

The battery bank consists of parallel 10kW/10kWh lithium-ion batteries. The voltage at maximum power point of the PV array is 59.1V, sufficient to recharge the lithium-ion battery bank up to 95% State-of-Charge, inside the plateau of the charge voltage characteristics. The charge current into the battery during simulation should not exceed the advised 120A by the battery manufacturer, considering ambient temperatures between 10-50°C. The maximum continuous discharge current of the selected $LiFePO_4$-Battery is then 50A. At this behaviour, the expected battery lifetime up to 70% of its remaining capacity is 7,000 cycles as per manufacturer datasheet. Hence, the battery is expected to be replaced multiple times during the 25-year system's operational life.

Utilizing excess electricity from renewable sources, e.g., Solar PV, renewable hydrogen can be produced via water electrolysis [38]. The on-site PEM electrolyser, consisting of parallel connected 5kW stacks, generates hydrogen which is stored in a Ti-based AB2 Solid-Hydrogen Storage Cell. The heat generated in the exothermic reaction is recovered in the recirculating cooling water circuit and utilized for heating of the Fuel Cell stack to reduce thermal cycling stresses and avoid cold start-ups, as well as pre-heating of the electrolyser water supply.

The RHFC Energy Storage System (ESS) is designed with a rated power capacity of 5kW to cover the 3.6kW peak load with 40% excess capacity. The proposed energy system can be modularly increased to act as a micro-grid and provide electricity to the rural community around. The PEM Electrolyser voltage is controlled between 1.6-2.2V/cell, equal to 22.4-30.8V per stack. In the parallel connection, the circuit voltage becomes 44.8 - 61.6V. The operating current for the stacks at these voltages is 10-220A, or 0.1 - 2.2A/$cm^2$.

Charging and discharge kinetics of the Ti-based AB2 metal-hydride are empirically tested by Dehouche et al. [24]in order to validate charging capacity, (dis-)charging equilibrium pressure ($P_{eq}$), cycling stability, and absorption and desorption kinetics [24]. The Pressure–composition–temperature (PCT) curve is shown in Figure 1, which shows that the nano-structured Ti-based AB2 can store up to 1.6 wt.% when

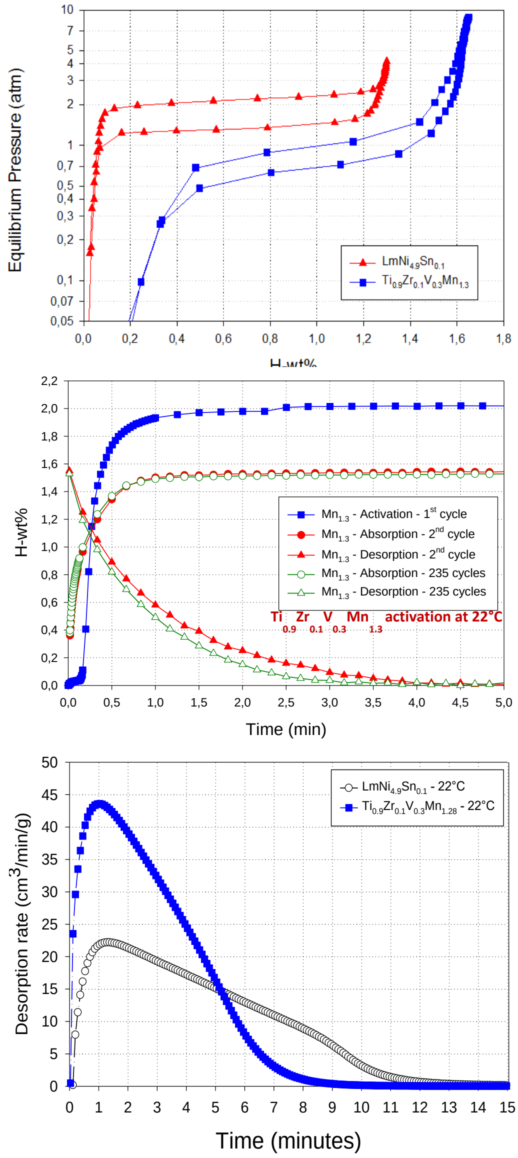


*Figure 1 - Characteristics and kinetics of the Ti-based AB2 Metal-Hydride, showing the equilibrium pressure for absorption and desorption (atm), desorption rate to satisfy PEM Fuel Cell hydrogen demand (cc/min/g), and the stability after 235 cycles [51]*

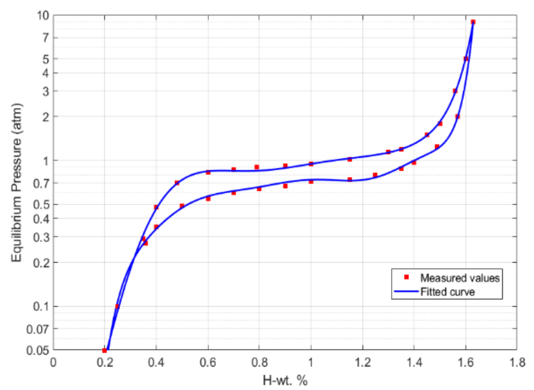


*Figure 2 - Levenberg-Marquardt curve fitting to the empirical metal-hydride results (figure 1) and utilising equation 18 and 19. The fit parameters are given in table 5.*

charged with below 10 bar of hydrogen pressure and after extensive cycling and offers good instantaneous discharge kinetics to allow for fast PEMFC start-up. These curves are used as input parameters for the simulations described in section 2.3. The lab results are fitted to the MATLAB/Simulink model using a Levenberg-Marquardt least square algorithm as shown in Figure 2, while the fitted parameters are presented in Table 4 in section 2.3. The plateau slopes are first determined for the values of H-wt.% between 0.5 and 1.2 and used as f(X) in equation 18 in order to find the enthalpy (ΔH) and entropy (ΔS) for absorption and desorption in the Van't Hoff equation 18. Thereafter, these values are used to identify the $a_i$ parameters of f(X) for absorption and desorption using equation 19.

A low temperature PEMFC is used to regenerate DC electricity from the stored hydrogen, as opposed to a high-temperature fuel cell [39] due to the commercial availability at the time of writing. PEMFC is perfectly suitable for backup power and distributed power generation because of its quick start-up time, low operating temperature and long lifetime. In theory, the process of a PEM fuel cell is the reversed of that of a PEM electrolyser. Hydrogen and air react to generate DC electricity, water and heat. To optimize balance-of-plant (BOP) and limit parasitic losses due to thermal energy requirements, the selected metal-hydride temperature characteristics should match the fuel cell operating temperature [40]. Liquid-cooled fuel cell is chosen for better control of the operating temperature [41], since the added weight is not significant in a stationary application, as opposed to applications such as Unmanned Aerial Vehicles [42]

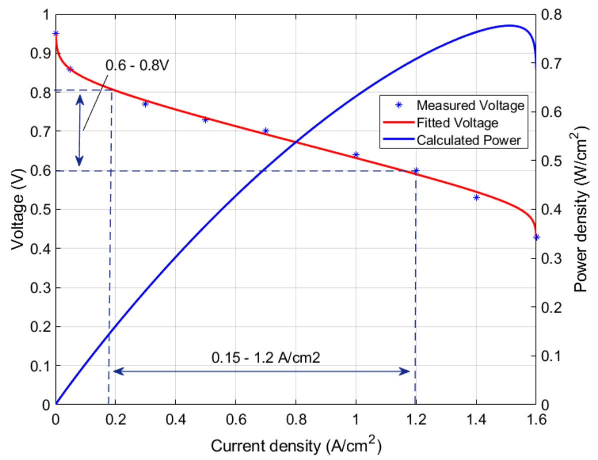


*Figure 3 - Levenberg-Marquardt fitting to the empirical PEMFC results and utilising equation 11-15. The fit parameters are given in table 6.*

The PEM Fuel Cell model is empirically validated in a lab environment and the Levenberg–Marquardt algorithm is used to fit the computational and empirical curves, replicating the expected real-life operating conditions as shown in Figure 3. The Fuel Cell is operated at 60°C cell temperature and inlet gas temperatures. Relative humidity of the reactant gases is 100% and mass flow rates are as per equation 16 with stoichiometric flow rates of 1.2 and 2 for hydrogen and air, respectively. The lab-scale PEM Fuel Cell utilizes a 25cm$^2$ Membrane Electrode Assembly with 0.4mg/cm$^2$ platinum loading and 5mm thick graphite bipolar plates with square cross-sectional area, 4-channel serpentine flow-field design. Results of the empirical testing and validation of the Simulink model is presented in Figure 3, while the fitted parameters are presented in Table 3. The operating voltage of the Fuel Cell is 0.6-0.8V/ cell as can be seen in Figure 8, or 21-28V for the 35 Cell stack. The current range of the Fuel Cell is 0.15-1.2A/cm$^2$, or 30-240A for the 200cm$^2$ active area. The total operational power range of the Fuel Cell is then 1.17kW - 5.04 kW. This operating strategy is chosen to avoid risks of premature degradation for operation in the mass concentration area, which potentially accelerates dissolution of Platinum/Carbon catalyst and hence shortens the Fuel Cells lifetime [43].

Hybridization with a Lithium-Ion battery pack also avoids high parasitic losses in the low current-density zone, where input power to auxiliary equipment to run the fuel cell, e.g., air blower, takes up a significant part of the power generated by the Fuel Cell, thereby significantly enhancing the system’s efficiency at low-power operation or during start-up of the RHFC. Additionally, this protects the Fuel Cell from running at potential range between 1 – 1.2 V/cell during rapid transient load changes, at which platinum is unstable according to the Pourbaix diagram [44].

The high-level control flow diagram is presented in Figure 4. The battery is used as primary backup for the renewables when the State of Charge is between 15% and 95%, and the Fuel Cell is used as secondary backup and can be discharged completely. In the case both are empty, a Loss-of-Load alarm is sent to the operator. When power generated by renewables exceeds the demand of the load, the battery is charged up to 95%, after which the electrolyser is powered to recharge the hydrogen. When hydrogen is recharged

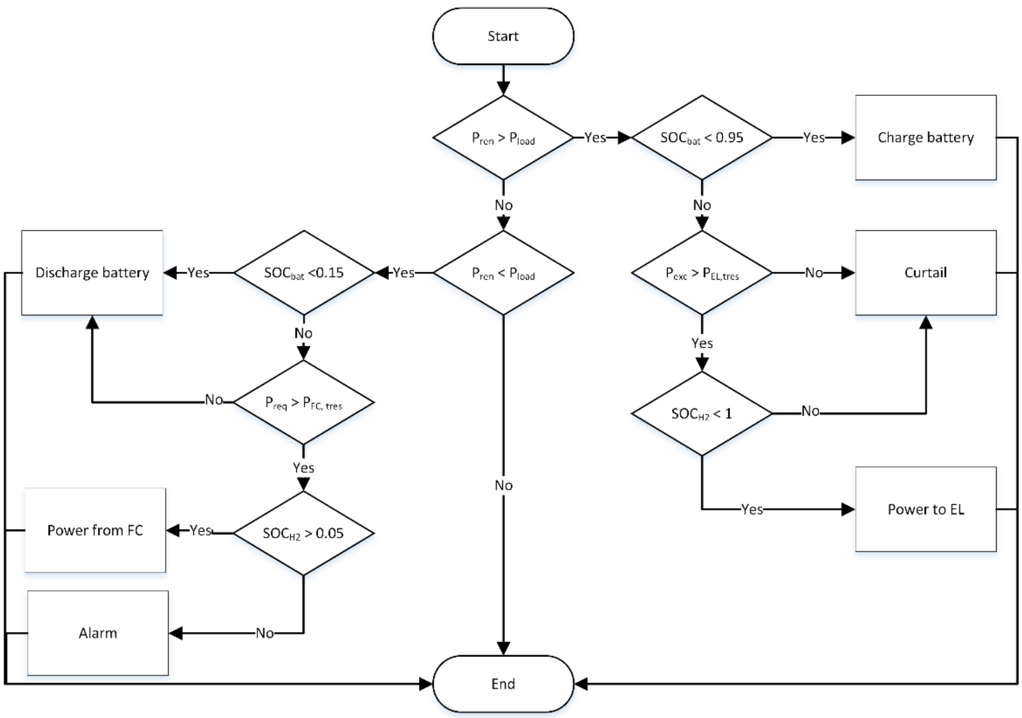


*Figure 4 - Control system flow diagram, showing the decision making and hierarchy of the system, where the battery is used as primary backup for the renewables when the State of Charge is between 15% and 95%, and the Fuel Cell is used as secondary backup and can be discharged completely. In the case both are empty, a Loss-of-Load alarm is sent to the operator. When power generated by renewables exceeds the demand of the load, the battery is charged up to 95%, after which the electrolyser is powered to recharge the hydrogen. When hydrogen is recharged completely, the renewables are disconnected, and their energy curtailed.*

completely, the renewables are disconnected at the MPPT controller and their energy is curtailed.

The typical telecommunication tower site operates of a -48VDC bus [45, 46], hence converters are required to connect the systems to the bus. The model is simulated in fixed timestep of 1 Hz with ODE3b solver. Therefore, capacitance, inductance and switching effects of converters are neglected and a 1D-lookup table, with efficiency values adapted from the findings regarding the interleaved boost converters of Youn et al. [47], is used to emulate the DC-DC converter efficiencies. As the system is not grid-connected, further small signals of DC/AC transformers and their effect on the fuel cell operation are disregarded [48]. A schematic design of this system can be found in Figure 11.

## 2.2 MATLAB/Simulink input data & boundary conditions

Data of the telecommunication tower electricity demand is measured in 15-minute intervals using an Autometers HC1 datalogger installed directly on the distribution panel to measure, besides others, the voltage, current, and the total power consumption as is presented in Figure 5. The electricity demand is measured over one month and extrapolated to represent the full year. The telecommunication tower load is a DC load, running at -48$V_{DC}$ with a power consumption between 2.2 and 3.6kW, averaging at 3.1kW. Additional reference data for the model is presented in Table 1.

*Table 1 - Data for modelling the single-tenant cell phone tower energy system.*

| **Reference data** | |
|---|---|
| Avg. solar irradiance | 276.8 W/m$^2$ |
| Avg. Sun Peak Hours | 5.9 h/day |
| Avg. ambient temperature | 24.1°C |
| Avg. site load | 3.1 kW |
| System design life | 25 years |
| Annual inflation | 2.3% |

## 2.3 Governing equations

The conversion efficiency of solar cells is influenced by the solar irradiation received and the cell temperature. Modules are connected in

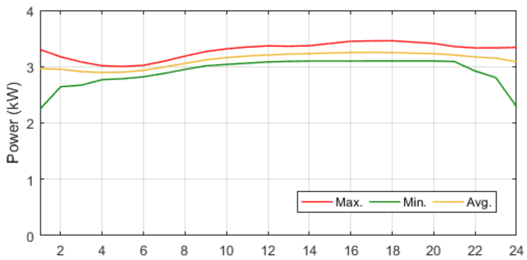


*Figure 5 - Measured load from single-tenant cell phone tower.*

series or parallel to form an array to achieve the desired current and voltage for the application. The cell operating current with changing irradiance and ambient temperature is calculated by [49]:

$$I_{PV} = I_{PH} - I_0 \left[ exp\left(\frac{V + IR_S}{nV_T}\right) - 1 \right] - I_{SH} \qquad (1)$$

Where the thermal voltage is found by [49]:

$$V_T = \frac{kT}{q} \qquad (2)$$

The temperature and irradiance corrected photocurrent is found by [49]:

$$I_{PH} = I_{SC} + K_i(T - T_{ref}) \cdot \frac{G}{1000} \qquad (3)$$

Manufacturing defects or improper design of the solar cell can cause significant power losses if low shunt resistance is present. A low shunt resistance in the solar cell creates an alternative pathway for the photo-current to flow, hence reducing the useable current in the system and decreasing the efficiency. The shunt current is expressed as [49]:

$$I_{SH} = \frac{\frac{V}{N_S} + IR_S}{R_{SH}} \qquad (4)$$

The temperature corrected dark saturation current is found by [49]:

$$I_0 = I_{RS} \left[\frac{T}{T_{ref}}\right]^3 exp\left[\frac{qE_{g0}}{nk}\left(\frac{1}{T} - \frac{1}{T_{ref}}\right)\right] \qquad (5)$$

The reverse saturation current, $I_{RS}$,is a measure of the leakage current between the anode and cathode of the solar cell, and thus is generated current not useable for work. The cell reverse saturation current is found by [49]:

$$I_{RS} = \frac{I_{SC}}{\left[exp\left(\frac{qV_{OC}}{N_S nkT}\right) - 1\right]} \quad (6)$$

The Solar PV sub-model is modelled after the SunPower X22-360 module, its main characteristics are shown in Table 2. Modules are connected in parallel to increase the current output of the Solar PV array.

*Table 2 - SunPower X22-360 data for simulation [30].*

| **Description** | **Details** |
|---|---|
| Short-circuit current ($\boldsymbol{I_{sc}}$) | 6.48 A |
| Open circuit voltage ($\boldsymbol{V_{oc}}$) | 69.5 V |
| Number of cells in series | 96 |
| Temperature coefficient ($\boldsymbol{K_i}$) | 2.9 mA/°C |
| Normal Operating Cell Temperature | 45°C |

The PEM electrolyser stack is modelled with respect to Faraday's law of electrolysis and the PEM electrolysis electrochemical reaction kinetics [50]. The principle of water electrolysis is:

$$2H_2O + Electricity + Heat \rightarrow 2H_2 + O_2 \quad (7)$$

Where electricity and heat depend on the operating conditions of the PEM electrolysis cell. According to Faraday's law of electrolysis, hydrogen production is directly proportional to the electric charge applied at the electrodes. The hydrogen production rate of a PEM electrolyser can therefore be expressed as [50]:

$$f_{H_2} = N_p \eta_f \frac{I}{nF} \quad (8)$$

In an electrolysis cell, electrons and ions can participate in unwanted side-reactions and reduce the cell efficiency. This Faraday efficiency of electrolysis can be found by [50]:

$$\eta_f = 96.5e^{\left(\frac{0.09}{i} - \frac{75.5}{i^2}\right)} \quad (9)$$

The applied electrical current to the electrodes is directly related to irreversible losses in the electrolyser and will increase the stack voltage and hence increase the power consumption of the electrolyser as per [50]:

$$V_{el} = V_{Nernst} + E_{act} + E_{ohm} + E_{conc} \quad (10)$$

The activation overpotential refers to the energy required to start the reduction and oxidation reactions in the electrochemical cell and is found by [50]:

$$E_{act} = -2.3\frac{RT}{\alpha F}\log(i_0) + \frac{RT}{\alpha F}\log(i) \quad (11)$$

The ohmic overpotential results from the internal resistance of the cell components and is found by [50]:

$$E_{ohm} = iR_i \quad (12)$$

At high current densities, the transport of reactants to the reaction sites can become limited and reduce the concentration, thereby reducing the cells potential. This concentration overpotential is found by [50]:

$$E_{conc} = \frac{RT}{nF}\ln\left(\frac{i_L}{i_L - i}\right) \quad (13)$$

A PEM fuel cell is used to regenerate DC electricity from the hydrogen stored. In theory, the process of a PEM fuel cell is the reversed of that of a PEM electrolyser. Hydrogen and air react to generate DC electricity, water and heat. The correlating equation of this process is [51]:

$$H_2 + \frac{1}{2}O_2 \rightarrow H_2O + Electricity + Heat \quad (14)$$

Like the PEM electrolyser, the amount of electricity and heat produced depends on the operating conditions of the PEM Fuel Cell. The PEM fuel cell consist of similar losses compared to the electrolyser as per equation 11-13, except in the fuel cell environment the voltage drops with increased current drawn as per [51]:

$$V_{FC} = V_{Nernst} - E_{act} - E_{ohm} - E_{conc} \quad (15)$$

The amount of hydrogen required is directly related to the current drawn from the fuel cell by [51]:

$$f_{H_2} = S \cdot \frac{I \times N_p}{n \times F} \quad (16)$$

For Fuel Cell and Electrolyser, different input variables for the operating parameters are required, an overview of these is presented in Table 3.

*Table 3 - Input variables for PEMFC and PEMEL model.*

| Parameter | Fuel Cell | Electrolyser |
|---|---|---|
| $\boldsymbol{\alpha}$ | 0.62 | 0.23 |
| $\boldsymbol{i_0}$ | 1.5*10$^{-4}$ A cm$^{-2}$ | 4.5*10$^{-2}$ A cm$^{-2}$ |
| $\boldsymbol{R_i}$ | 0.16 Ω cm$^{-2}$ | 0.21 Ω cm$^{-2}$ |
| $\boldsymbol{i_L}$ | 1.6 A cm$^{-2}$ | 2.2 A cm$^{-2}$ |
| $\boldsymbol{N_s}$ | 18 | 30 |
| **Active area** | 200 cm$^2$ | 100 cm$^2$ |
| **Temperature** | 65°C | 60°C |

Hydrogen generated by the electrolyser is stored in a Solid-Hydrogen Storage Cell. Metal-Hydride storage uses a reversible chemical process reaction between the nanostructured solid-alloy and hydrogen gas. Hydrogen gas is absorbed into the crystal-structure of the alloy to form a metal-hydride according to the expression:

$$M + \frac{x}{2} H_2 \leftrightarrow MH_x + \Delta H \quad (17)$$

Where $x$ can vary depending on material characteristics, preparation, and activation. The gas-solid phase equilibrium pressure ($P_{eq}$) is described by the van't Hoff's equation corrected by the hydrogen-to-metal ratio ($f(X)$) [52]:

$$\ln\left(\frac{P_{eq}}{P_0}\right) = \frac{\Delta H}{RT} - \frac{\Delta S}{R} + \text{f(X)} \quad (18)$$

The quantities $\Delta H$ and $\Delta S$ vary with alloy composition and have different values for absorption and desorption due to hysteresis. $f(X)$ is expressed by the following general form, the values for $a_i$ can be found in Table 4.

$$\text{f(X)} = \sum_{i=1}^{9} a_i tan^i \pi\left(\frac{X}{X_{max}} - \frac{1}{2}\right) \quad (19)$$

*Table 4 - Values of the coefficients for metal-hydride.*

| | Absorption | Desorption |
|---|---|---|
| **ΔH** | -34,120 J/mol | - 34,470 J/mol |
| **ΔS** | -115.16 J/mol·K | -113.48 J/mol·K |
| $\boldsymbol{a_1}$ | 1.4577 x 10$^{-1}$ | 3.7670 x 10$^{-1}$ |
| $\boldsymbol{a_2}$ | 1.8136 | 4.2464 x 10$^{-1}$ |
| $\boldsymbol{a_3}$ | -1.4743 | -7.2843 |
| $\boldsymbol{a_4}$ | -4.8656 x 10$^{1}$ | 6.6114 x 10$^{1}$ |
| $\boldsymbol{a_5}$ | 1.5159 x 10$^{2}$ | 2.4799 x 10$^{2}$ |
| $\boldsymbol{a_6}$ | -8.6125 x 10$^{1}$ | 8.3607 x 10$^{2}$ |
| $\boldsymbol{a_7}$ | -6.6868 x 10$^{2}$ | -2.2442 x 10$^{3}$ |
| $\boldsymbol{a_8}$ | 1.9901 x 10$^{2}$ | -3.7422 x 10$^{3}$ |
| $\boldsymbol{a_9}$ | 9.2057 x 10$^{2}$ | -8.6533 x 10$^{3}$ |

## 2.4 Economic assessment

With many emerging energy technologies, business face many competing investment opportunities. To compare investment opportunities on a like-for-like basis, the most effective methods discount future net cash inflows, and further capital outflows back to their equivalent Net Present Value (NPV). The NPV represents the value or contribution of an investment to the business. If the NPV is positive, the investment is potentially worthwhile [53].

$$\text{NPV} = -\text{C}_0 + \frac{C_1 + M_1 + F_1}{1 + R} + \cdots + \frac{C_T + M_T + F_T}{(1 + R)^T} \quad (20)$$

The IRR uses discounted cash flows to calculate a percentage rate of return on an investment as per equation 21. The IRR can be more conceptually benchmarked against other investment returns as compared to the NPV [53].

$$0 = \text{NPV} = \sum_{t=1}^{n} \frac{C_n}{(1 + IRR)^n} \quad (21)$$

The LCOE is an important financial parameter to measure cost-effectiveness of energy generating technologies. Although LCOE calculations are

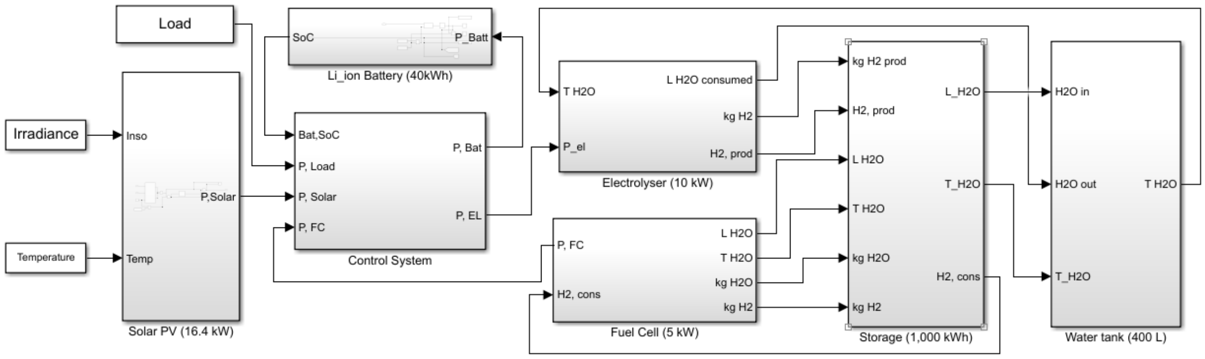


*Figure 6: MATLAB/Simulink of the integrated hybrid renewable energy micro-grid system. Installed capacities are adjustable to configure future studies with different load profiles.*

sensitive to the underlying data, it offers a comparison between projects and technologies. LCOE aims to provide comparisons of different technologies with different project size, lifetime, different capital cost, return, risk, and capacities. It is an economic assessment of the total cost to build and operate a power-generating asset over its lifetime divided by the total energy output of the asset over that lifetime [54]. The LCOE is calculated by:

$$LCOE\ (\frac{\$}{kWh}) = \frac{\sum_{t=1}^{n} C_t + M_t + F_t\ (\$)}{\sum_{t=1}^{n} E_t\ \ (kWh)} \qquad (22)$$

Which covers the whole lifetime of the energy system from year 1 ($t = 1$) to end of life ($t = n$). Where, $C_t$ is the CAPEX, $M_t$ is the OPEX, $F_t$ is the fuel cost, and $E_t$ is the electricity generated by the system. CAPEX and OPEX are gathered from industry reports and peer reviewed journal articles where possible and are presented in Table 5 and 6, respectively.

*Table 5 - Capital expenditures for selected technologies.*

| | |
|---|---|
| Solar PV | $1,250 per kW |
| Li-Ion battery storage capacity [55] | $390 per kWh |
| Li-Ion battery power capacity [55] | $400 per kW |
| RHFC electrolyser capacity [12] | $1,800 per kW |
| RHFC storage capacity [56] | $20 per kWh |
| RHFC power capacity [57] | $2,000 per kW |
| Diesel Genset [58] | $600 per kW |

*Table 6 - Operation and Maintenance expenditures for selected technologies.*

| | |
|---|---|
| Solar PV | 1.2% of CAPEX |
| Li-Ion battery variable [55] | $0.003 per kWh |
| Li-Ion battery fixed [55] | $10 per kW |
| RHFC electrolyser variable | $0.02 per kWh |
| RHFC storage | 0.5% of CAPEX |
| RHFC fuel cell variable | $0.02 per kWh |
| Diesel Genset [59] | $0.78 per op. hour |

# 3. Results and discussion

The modelling and simulation of the carbon-free energy system in MATLAB/Simulink environment is performed with the aim of optimizing its economic performance using an iterative process varying installed capacities. The results show the modelled energy system and the economic performance as well as the technical design to power a single tenant, off-grid telecommunication tower.

## 3.1 Modelling results

The governing equations outlined in section 2.2 are modelled in MATLAB/Simulink environment, resulting in the model presented in Figure 6. The Solar PV model calculates the voltage, current, and resulting power generated by the Solar PV array from the hourly temperature and irradiance data. The solar module model itself is adjustable to fit commercial Solar PV module performance by adjusting the $V_{OC}, I_{SC}, N_P$ etc. Solar PV electricity generation and load demands are fed into the control system to determine the discrepancy between demand and supply. The control system determines, based on Li-Ion and $H_2$ storage state-of-charge (SoC), whether to store or discharge energy from the ESS's battery and/or RHFC module. The Lithium-Ion battery's charge capacity and nominal voltage can be amended, as well as the charge- and discharge capacities. In the RHFC, the mass of Ti-based AB2 material can be amended to change the storage capacity, as well as the Electrolyser and Fuel cell active areas and number of cells the stack are configurable.

Figure 7 shows the simulation outcomes for the week of 9-16 October. During the day, Solar PV generates sufficient electricity to power the load and excess electricity is sent to the Li-Ion battery pack and/or electrolyser, indicated as negative energy flow in Figure 7. At night, when Solar PV is not available, the Li-Ion battery pack is used up

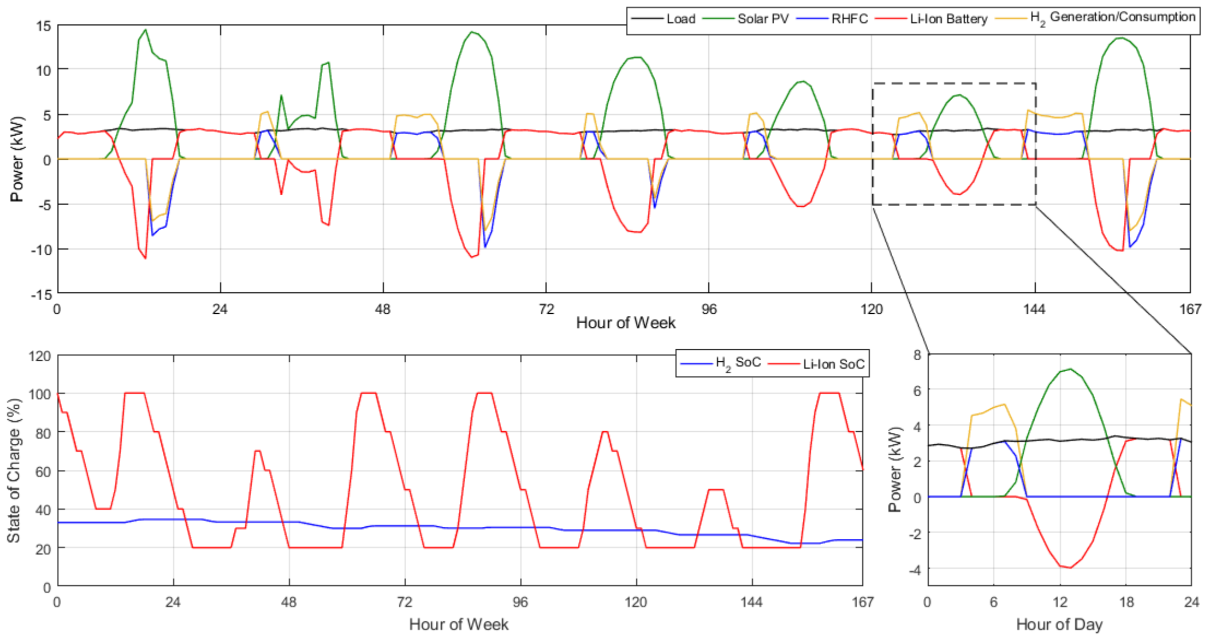


*Figure 7 - Dynamics of the energy system, showing the ability to respond to demand chances. When renewable energy is available, this is sent to power the load. When there is an excess of renewable energy generated, this is sent to the Li-Ion battery, as well as the PEM electrolyser to produce hydrogen (H2), as is visible when the Li-Ion and hydrogen charge is represented by a 'negative discharge'. When renewable energy generation is not sufficient to power the load, the PEM Fuel Cell covers the load requirements.*

to 80% Depth-of-Discharge (15-95% SOC), after which the Fuel Cell satisfies the load demand.

The operation is simulated over a full year to be able to examine system responses and load sharing between the solar PV, battery, and RHFC under various conditions. From Figure 10, it can be seen that the RHFC backup is critical throughout the year, when reduced Sun Peak Hours limit the battery recharge capacity and the RHFC share to power the load is over 40% of the total daily energy demand.

When water recovery loop is not installed, a 1,700L water tank would be required to prevent excessive site visits to remote locations as is shown in the accumulated water consumption in

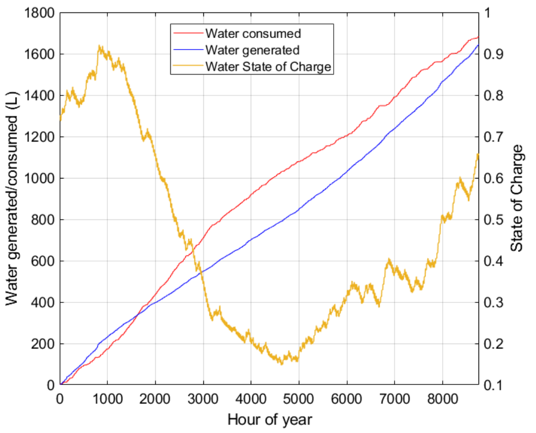


*Figure 8 - Accumulative water produced and consumed during the year, and corresponding State-of-Charge.*

Figure 8. However, significant water refill of 1,700L per year is still required in that case, in areas prone to lack clean water supply. With the thermal integration and water recirculation, the tank size can be limited to 400L tank, and no external water source or additional site visits are required, providing further benefits to the autonomous operability of the system.

The system efficiency is evaluated by the average round-trip efficiency of the Battery and RHFC including dynamic convertors losses over the

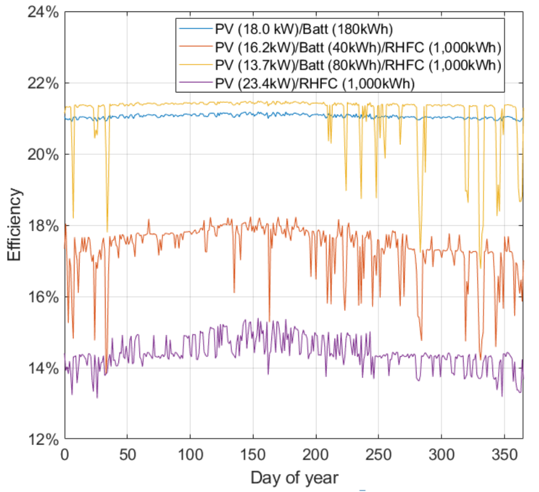


*Figure 9 - System efficiency of the analysed energy system configurations, showing high energy efficiency in the battery-only backup system (Batt) and a drop in efficiency when RHFC is added to the system, particularly during days of high PEMFC utilisation.*

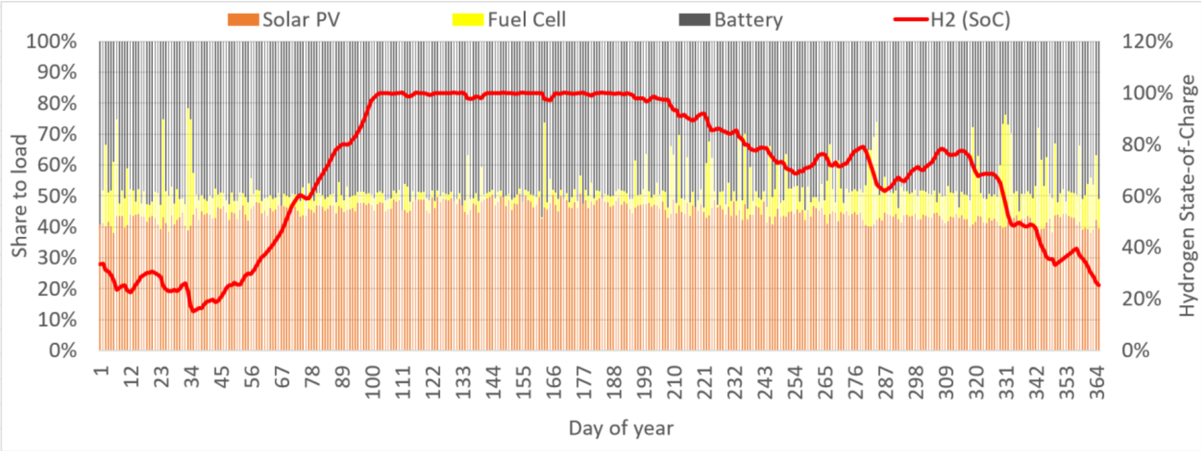


*Figure 10 - Daily share of electricity delivered to the load, showing critical fuel cell backup during prolonged periods of low solar irradiance and/or high load demand. Hydrogen generation and seasonal storage offer the advantage of energy storage during periods of high solar irradiance and utilization during periods of low solar irradiance, allowing the RHFC to provide a share of over 40% of the total daily energy demand.*

year, as well as the Solar PV conversion efficiency and plotted to represent a daily average system efficiency based on the share of power to the load. With only Solar PV and battery, the system achieves the highest overall efficiency of 21.05% due to the relatively even share to power the load of 43.94% vs. 56.06%, respectively, combined with high individual efficiencies of 22.18% and 90.28%, respectively. It is evident that efficiency drops when a larger share of the load is powered by the RHFC, directly linked to the lower RTE of the RHFC (between 33.14% - 37.84% in the analysed cases) versus that of the battery (between 88.24% - 93.11%). This results in a system efficiency of only 14.41% for the Solar PV/RHFC system. The combined system efficiency at each day of the year is shown in Figure 9.

## 3.2 Energy system design results

As is shown in Figure 11, the proposed energy system is further designed to represent the full site considerations. Besides the earlier discussed energy components such as the Solar modules, battery and RHFC, also the necessary safety components are included in this schematic. Residual Current Devices are installed in each circuit to protect the circuit from current mismatch between live and neutral wires and cut the circuit in case such event happens. To protect the circuit from overcurrent and/or short-circuit, Main Circuit Breakers are in place in each individual circuit and are sized to trip if 20% overcurrent occurs in the respective circuit. Diodes are in place in the Solar PV array and RHFC circuits to protect components from damage due to reverse current. To ensure optimal system efficiency, resistive losses should be limited through proper wire sizing. Improper sizing of wires increases the voltage drop over the wire length or through uncontrolled resistive heating of the wires, causing wire failure or fire hazards.

## 3.3 Financial results

Any investment carries risks and requires extensive evaluation of the expected benefits to make a rational decision and mitigate the financial risks of the investment. To compare the several system configurations and optimize the return on the initial investment, the Net Present Value and IRR have been calculated and plotted as a function of the battery capacity in Figure 12. Figure 12 also presents the CAPEX and LCOE of the system configurations. From the figure, the influence on battery capacity on the economic performance of the hybrid energy storage system is clearly visible. The capital cost of installation is lowest with battery capacity of 40kWh, as the higher round-trip efficiency (RTE) reduces the installed capacity of Solar PV from 23.4 kW for a Solar PV/RHFC system to 16.2 kW. However, higher battery capacities offset the advantage of reduced capital cost related to the installed capacity of Solar PV. The LCOE is most cost-effective with a 40kWh battery capacity at 17.16 c/kWh, as the hybridization at this scale allows for lowest total CAPEX and OPEX and achieves sufficient high system efficiency to effectively deliver the energy to the load. This means that for the most cost-effective system, the system efficiency is relatively low at 17.33% as described in section 3.1, hence a high system efficiency does not directly translate to economic feasibility. The LCOE significantly increases with increased battery capacity, predominantly influenced by the

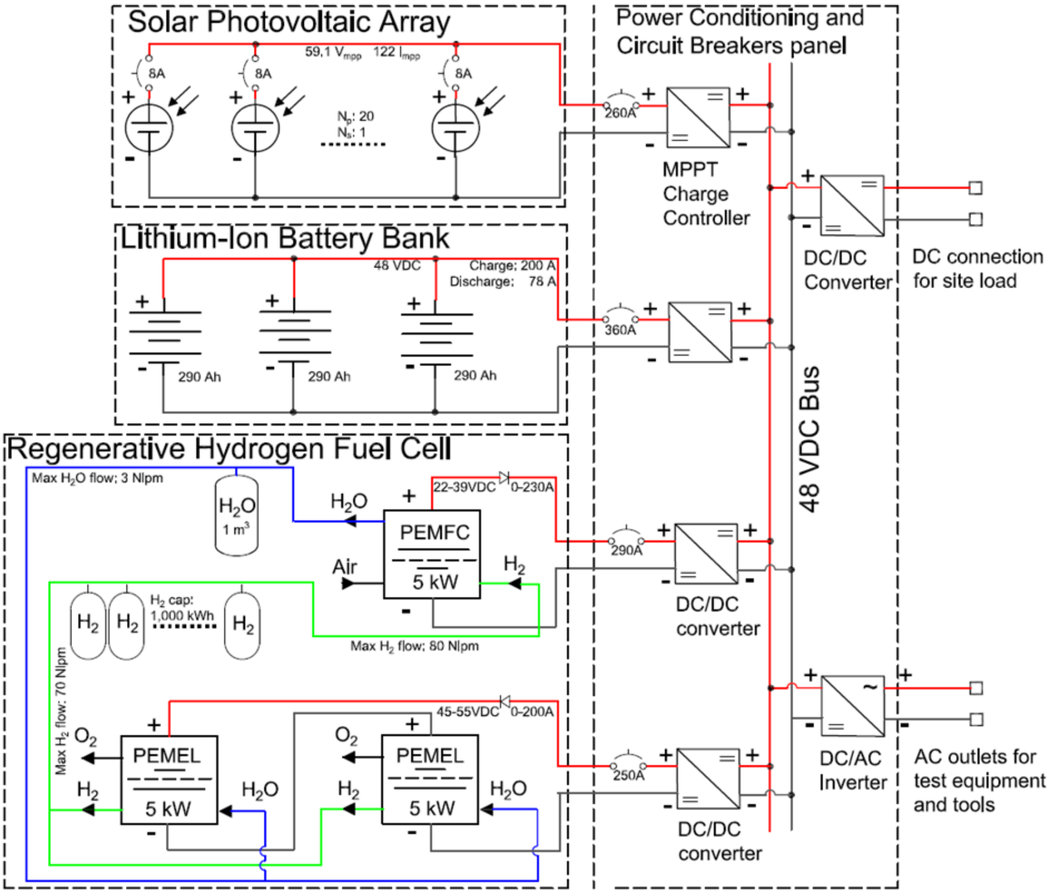


*Figure 11 - Schematic of the proposed energy system consisting of parallel 45 Solar PV modules for primary power supply, 40 kWh battery storage, two 5kW PEM Electrolyser stacks to generate hydrogen from excess Solar PV, Ti-based AB2 Solid-Hydrogen energy storage, and a 5kW PEM Fuel Cell for backup power generation.*

battery replacement cost, up to 47.01 c/kWh at 160kWh battery capacity in the hybrid ESS and slightly reduces to 40.00 c/kWh for a Solar PV/Battery system. The RHFC dominated ESS configurations achieve a positive NPV, indicating the RHFC is critical in achieving commercial viability of the system. From Figure 12 it can be seen that operational cost of a hybrid or RHFC ESS are significantly lower compared to a battery ESS, almost completely due to an increase in variable O&M which include battery capacity increases the cost-effectiveness of the hybrid ESS up to the point that the relatively low RHFC RTE hurts the operational system efficiencies and increased Solar PV installed capacity is critical to offset the energy losses in the RHFC. The IRR follows a similar trend as the NPV; however, the IRR is marginally lower for

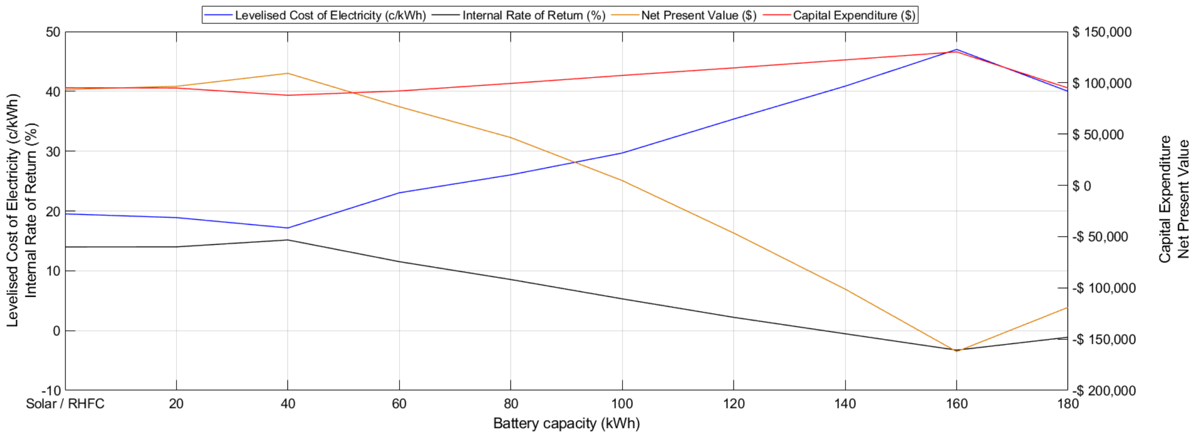


*Figure 12 - Influence of battery sizing on the Levelised Cost of Electricity, capital cost, and Solar PV required capacity, showing a system consisting of 16.2kW Solar PV, 40kWh Lithium-Ion battery, 10kW electrolyser, 1,000kWh solid-hydrogen energy storage, and 5kW Fuel Cell to be most cost-effective solution for a single tenant off-grid telecommunication tower.*

the 20kWh system (15.15% vs. 14.00%, respectively). This is attributed to the lower CAPEX of the 20kWh system ($87,850 vs. $94,900, respectively). From Figure 12, it is evident that the RHFC has a significant impact on the LCOE for a single tenant telecommunication tower compared to battery or diesel-based systems, mainly contributed to the low OPEX. Combining a battery and RHFC as backup further reduces the LCOE, by reduced CAPEX of the system. Thereby, it can improve reliability and longevity of the system by reducing the annual operating hours of each technology, avoiding deep discharge of the battery pack, and avoiding excessive cycling stresses in the battery and RHFC.

## 4. Conclusion

The article establishes a strong evidence-based data set and formulate possible integration options using optimised empirical parameters and detailed modelling work to provide an outline design for a hybrid, integrated, and off-grid clean energy system, designed to provide a strong and resilient business model by understanding the relationship between the system's capacity design, operational efficiency, and economic performance to show commercial feasibility of the technology. Extensive simulations have been performed in MATLAB/Simulink environment, and Levenburg-Marquardt least square algorithm is used to identify thermodynamic parameters and empirically validate the Solid-Hydrogen Storage Cell and PEM Fuel Cell. The proposed optimized energy system contains an energy mix of 16.2 kW Solar PV for primary power generation coupled to a 10kW/40kWh Li-Ion battery for short duration energy storage and an RHFC (consisting of a 10kW PEM Electrolyser, 1,000kWh Ti-based AB2 Solid-Hydrogen Storage Cell, and 5kW PEM Fuel Cell) for long duration energy storage in a -48VDC nano-grid topology. The results show a reduced need for site-visits related to water and/or fuel delivery, as well as enhanced cost-effectiveness of the synergized system despite achieving lower overall system efficiency of 17.33% vs. 21.05% for a Solar PV/Battery system, resulting in an LCOE of 17.16 ¢/kWh compared to 73.40 ¢/kWh for a Diesel Genset power telecommunication tower. With a Net Present Value of $109,235 and IRR of 15.15%, the investment has commercial viability. Therefore, the initial high capital cost become valuable investment through reduced operational expenditures increasing the MNO's profits in the long term, as well as increasing energy security, equity, and sustainability.

Based on the financial analysis of the ESS configurations, it is advisable to hybridise ESS to achieve optimum return on the capital investment and limit financial risks while satisfying single tenant telecommunication load demand with zero on-site $CO_2$ emissions. The results of the parametrisation of the metal-hydride and fuel cell, as well as the holistic techno-economical case study methodology will be of interest to future researchers in this field, while the results on the importance of hybridisation provide a direction for future research in hybrid zero-emission energy systems and acceptance of hydrogen as an energy storage technology, in particular for off-grid applications. Future work will include modelling and simulating using real-time data to evaluate system behaviour during instantaneous responses to load changes and provide a platform for development of a Digital Twin model, as well as the development of a lab-scale prototype to validate the simulated energy and exergy efficiencies.


## Acknowledgement

This study is sponsored by and carried out in collaboration with SolarBotanic Ltd. We are grateful to IHS Towers NG Ltd. and Arqiva Group Ltd. for the valuable discussions related to the best options for integration and operation aspects.


## References


[1] Groupe Speciale Mobile Association. The Mobile Economy West Africa 2018. London: GSM Association; 2018.

[2] Aker JC, Mbiti I. Mobile Phones and Economic Development in Africa. J Econ Perspect. 2010;24:207-232. https://doi.org/10.1257/jep.24.3.207.

[3] Chavula HK. Telecommunications development and economic growth in Africa. Inf. Technol. Dev. 2013;19:5-23. https://doi.org/10.1080/02681102.2012.694794.

[4] Groupe Speciale Mobile Association. The Mobile Economy Sub-Saharan Africa. London, GSM Association; 2018.

[5] Groupe Speciale Mobile Association. Green power for mobile: The Global Telecom Tower Esco Market: Overview of

the global market for energy to telecom towers in off-grid and bad-grid areas. London, GSM Association; 2014.

[6] Laumbach RJ, Kipen HM. Respiratory Health Effects of Air Pollution: Update on Biomass Smoke and Traffic Pollution. J Allergy Clin Immunol. 2012;129:3-11. https://doi.org/10.1016/j.jaci.2011.11.021.

[7] Olatomiwa L, Mekhilef S, Nuda ASN, Sanusi K. Techno-economic analysis of hybrid PV–diesel–battery and PV–wind–diesel–battery power systems for mobile BTS: the way forward for rural development. Energy Sci. Eng. 2015;3:271-285. https://doi.org/10.1002/ese3.71.

[8] Oviroh PO, Jen T. The Energy Cost Analysis of Hybrid Systems and Diesel Generators in Powering Selected Base Transceiver Station Locations in Nigeria. Energies. 2018;11:1-20. https://doi.org/10.3390/en11030687.

[9] Groupe Speciale Mobile Association. Tower Power Africa: Energy Challenges and Opportunities for the Mobile Industry in Africa. London, GSM Association; 2014.

[10] Crouch M. Fuel Cell Systems for Base Stations: Deep Dive Study London, GSM Association; 2011.

[11] Khan MJ, Yadav AK, Mathew L. Techno economic feasibility analysis of different combinations of PV-WindDiesel-Battery hybrid system for telecommunication applications in different cities of Punjab, India. Renew. Sust. Energ. Rev. 2017;76:577-607. https://doi.org/10.1016/j.rser.2017.03.076.

[12] Schmidt O, Gambhir A, Staffell I, Hawkes A, Nelson J, Few S. Future cost and performance of water electrolysis: An expert elicitation study. Int. J. Hydrog. Energy. 2017;42:30470-30492. https://doi.org/10.1016/j.ijhydene.2017.10.045.

[13] Kumar A, Singh T, Singh S, Liu Y. A Comprehensive Review of Fuel Cell and its Types. Int. J. Mech. Eng. Technol. 2013;3:13-21. ISSN : 2249-5762.

[14] Ma Z, Eichman J, Kurtz J. Fuel cell backup power system for grid service and micro-grid in telecommunication applications. J. Energy Resour. Technol. 2019;141:062002. https://doi.org/10.1115/1.4042402.

[15] Amutha M, Rajini V. Techno-economic evaluation of various hybrid power systems for rural telecom. Renew. Sust. Energ. Rev. 2015;43:553-561. https://doi.org/10.1016/j.rser.2014.10.103.

[16] Serincan MF. Reliability considerations of a fuel cell based backup power system for telecom applications. J. Power Sources. 2016;309:66-75. https://doi.org/10.1016/j.jpowsour.2016.01.083.

[17] Scamman D, Newborough M, Bustamante H. Hybrid hydrogen-battery systems for renewable off-grid telecom power. Int. J. Hydrog. Energy. 2015;40:13876-13887.

[18] Guinot B, Champel B, Montignac F, Lemaire E, Vannucci D, Sailler S, Bultel Y. Techno-economic study of a PV-hydrogen-battery hybrid system for off-grid power supply: Impact of performances' ageing on optimal system sizing and competitiveness. Int. J. Hydrog. Energy. 2015;40:623-632.

[19] Gupta R. Hydrogen Fuel: Production, Transport, and Storage. Boca Raton: CRC Press; 2008.

[20] Abe JO, Popoola API, Ajenifuja E, Popoola OM. Hydrogen energy, economy and storage: Review and recommendation. Int. J. Hydrog. Energy. 2019;44:15072-15086. https://doi.org/10.1016/j.ijhydene.2019.04.068.

[21] Zhang J, Fisher TS, Ramachandran PV, Gore JP, Mudawar I. A Review of Heat Transfer Issues in Hydrogen Storage Technologies. J. Heat Transfer, 2005;127:1391-1399. https://doi.org/10.1115/1.2098875.

[22] Klebanoff L, Hydrogen Storage Technology: Materials and Applications. Boca Raton: CRC Press; 2013.

[23] Shokano G, Dehouche Z, Galey B, Postole G. Development of a Novel Method for the Fabrication of Nanostructured Zr (x) Ni (y) Catalyst to Enhance the Desorption Properties of MgH2. Catalysts. 2020;10:849-864. https://doi.org/10.3390/catal10080849.

[24] Dehouche Z, Savard M, Laurencelle F, Goyette J. Ti–V–Mn based alloys for hydrogen compression system. J. Alloys Compd. 2005;400:276-280. https://doi.org/10.1016/j.jallcom.2005.04.007.

[25] Cherrad N, Selloum D, Tingry S. Modeling the control of the desorption rate of hydrogen released from the adsorption storage bed to supply a fuel cell. Int. J. Hydrog. Energy. 2020;45:17605-17612. https://doi.org/10.1016/j.ijhydene.2020.04.120.

[26] Rusman N, Dahari M. A review on the current progress of metal hydrides material for solid-state hydrogen storage applications. Int. J. Hydrog. Energy. 2016;41:12108-12126. https://doi.org/10.1016/j.ijhydene.2020.04.120.

[27] Chen Z, Ma Z, Zheng J, Li X, Akiba E, Li HW. Perspectives and challenges of hydrogen storage in solid-state hydrides. Chin. J. Chem. Eng. 2020. In press. https://doi.org/10.1016/j.cjche.2020.08.024.

[28] Dehouche Z, Grimard N. Nanocomposite materials for hydrogen storage. In: Reese JP. New Nanotechnology Research. Gauthier: Nova Science Publishers, Inc; 2006. p. 2-64.

[29] International Renewable Energy Agency. Planning and prospects for renewable power: West Africa. Abu Dhabi: International Renewable Energy Agency, 2018. ISBN : 978-92-9260-081-5.

[30] SunPower. SunPower X-Series: X22-360-COM. 2017. http://spectrum.sunpower.com/sites/default/files/uploads/resources/X22_360COM_UK_AU_MC4Comp.pdf. (Accessed 12 06 2019).

[31] Muthuvel P, Daniel SA, Paul SK. Sizing of PV array in a DC nano-grid for isolated households after alteration in time of consumption. Eng. Sci. Technol. an Int. J. 2017;20:1632-1641. https://doi.org/10.1016/j.jestch.2017.12.006.

[32] Ballard. Fuel Cells: An Effective Rooftop Backup Power Solution. Burnaby: Ballard Power Systems Inc.; 2015.

[33] Osmotherly K. Batteries represent 40-50% of site capex: are you choosing the right ones? 2014. http://www.trojanbattery.com/pdf/TowerXchange_TrojanBattery.pdf (accessed April 4, 2019).

[34] Groupe Speciale Mobile Association. Powering Telecoms: West Africa Market Analysis. Sizing the Potential for Green Telecoms in Nigeria and Ghana. London: GSM Association; 2013.

[35] Parra D, Valverde L, Pino JF, Patel MK. A review on the role, cost and value of hydrogen energy systems for deep decarbonisation. Renew. Sust. Energ. Rev. 2019;101:279-294. https://doi.org/10.1016/j.rser.2018.11.010.

[36] Benlahbib B, Bouarroudj N, Mekhilef S, Abdeldjalil D, Abdelkrim T, Bouchafaa F, Iakdhari A. Experimental investigation of power management and control of a PV/wind/fuel cell/battery hybrid energy system microgrid. Int. J. Hydrog. Energy. 2020;45:29110-29122. https://doi.org/10.1016/j.ijhydene.2020.07.251

[37] Puranen P, Kosonen A, Ahola J. Technical feasibility evaluation of a solar PV based off-grid domestic energy system with battery and hydrogen energy storage in northern climates. Sol Energy. 2021;213:246-259. https://doi.org/10.1016/j.solener.2020.10.089.

[38] Turner J, Sverdrup G, Mann MK, Maness PC, Kroposki B, Ghirardi M, Evans RJ, Blake D. Renewable hydrogen production. Int. J. Energy Res. 2007;32:379-407. https://doi.org/10.1002/er.1372.

[39] Nazar K, Jaffery MH, Shakir I, Nazar A, Raza R. Design of 1 kW high temperature PEM fuel cell system and performance analysis under different operating conditions. Curr Appl Phys. 2020. In press. https://doi.org/10.1016/j.cap.2020.05.005.

[40] Lototskyy MV,Tolj I, Pickering L, Sita C, Barbir F, Yartys V. The use of metal hydrides in fuel cell applications. Prog. Nat. Sci. 2017;27:3-20. https://doi.org/10.1016/j.pnsc.2017.01.008.

[41] Chen Q, Zhang G, Zhang X, Sun C, Jiao K, Wang Y. Thermal management of polymer electrolyte membrane fuel cells: A review of cooling methods, material properties, and durability. Appl. Energy. 2021;286:116496. https://doi.org/10.1016/j.apenergy.2021.116496.

[42] Depcik C, Cassady T, Collicott B, Burugupally SP, Li X, Alam SS, Arandia JR, Hobeck J. Comparison of lithium ion Batteries, hydrogen fueled combustion Engines, and a hydrogen fuel cell in powering a small Unmanned Aerial Vehicle. Energy Convers. Manag. 2020;207:112514. https://doi.org/10.1016/j.enconman.2020.112514.

[43] Zhang S, Yuan XZ, Hin JNC, Wang H, Friedrich KA, Schulze M. A review of platinum-based catalyst layer degradtation in proton exchange membrane fuel cells. J. Power Sources. 2009;194:588-600. https://doi.org/10.1016/j.jpowsour.2009.06.073.

[44] Fuller T. Proton Exchange Membrane Fuel Cells 6. Pennington: The Electrochemical Society Inc.; 2006.

[45] Balshe W. Power system considerations for cell tower applications. Cummins Power Generation Inc.; 2011.

[46] Pal NK, Ifeanyi BJ. Technival overview of all sources of electrical power used in BTS's in Nigeria. Int. J. Eng. Res. Technol. 2017;4:18-30.

[47] Youn HS, Yun DH, Lee WS, Lee IO. Study on Boost Converters with High Power-Density for Hydrogen-Fuel-Cell Hybrid Railway System. Electronics. 2020;9:771. https://doi.org/10.3390/electronics9050771.

[48] Moazeni F, Khazaei J. Electrochemical optimization and small-signal analysis of grid-connected polymer electrolyte membrane (PEM) fuel cells for renewable energy integration. Renew. Energ. 2020;155:848-861. https://doi.org/10.1016/j.renene.2020.03.165.

[49] Nguyen XH, Nguyen MP. Mathematical modeling of photovoltaic cell/module/arrays with tags in Matlab/Simulink. Environ. Syst. Res. 2015;4. https://doi.org/10.1186/s40068-015-0047-9.

[50] Carmo M, Fritz DL, Mergel J, Stolten D. A comprehensive review on PEM water electrolysis. Int. J. Hydrog. Energy. 2013;38:4901-4934. https://doi.org/10.1016/j.ijhydene.2013.01.151.

[51] Jansen G, Dehouche Z, Corrigan H, Bonser R. An autonomous solar PV/Wind/Regenerative Hydrogen Fuel Cell energy storage system for cell towers. In: Shao H. Hydrogen Storage: Preparation, Applications and Technologies. Nova Science; 2018. p. 225-266.

[52] Dehouche Z, de Jong W, Willers E, Isselhorst A, Groll M. Modelling and simulation of heating/air-conditioning systems using the multi-hydride-thermal-wave concept. Appl. Therm. Eng. 1998;18:457-480. https://doi.org/10.1016/S1359-4311(97)00043-4.

[53] Warner S, Hussain S. The Finance Book. Harlow: Pearson Education Ltd.; 2017.

[54] Lai CS, McCulloch MD. Levelized cost of electricity for solar photovoltaic and electrical energy storage. Appl. Energy 2017;190:191-203. https://doi.org/10.1016/j.apenergy.2016.12.153.

[55] Aquino T, Roling M, Baker C, Rowland L. Battery Energy Storage Technology Assessment. Fort Collins: Platte River Power Authority; 2017.

[56] U.S. Department of Energy. Hydrogen Storage. 2017. https://energy.gov/eere/fuelcells/hydrogen-storage. (Accessed 27 04 2017).

[57] Battelle. Manufacturing Cost Analysis of PEM Fuel Cell Systems for PEM Fuel Cell Systems for Applications. Columbus: Battelle Memorial Institute; 2016.

[58] Baurzhan S, Jenkins GP. Off-grid solar PV: Is it an affordable or appropriate solution for rural electrification in Sub-Saharan African countries. Renew. Sustain. Energy Rev. 2016;40:1405-1418. https://doi.org/10.1016/j.rser.2016.03.016.

[59] HOMER. HOMER Energy Report. 2016. http://usersupport.homerenergy.com/customer/en/portal/articles/2188634-diesel-o-m-costs. (Accessed 24 04 2017).

907